Enhancement of the annihilation of dark matter in a radiative seesaw model

arXiv:1002.3225v2 [hep-ph] 27 Jul 2010

Enhancement of the annihilation of dark matter in a radiative seesaw model

Daijiro Suematsu[*], Takashi Toma[†] and Tetsuro Yoshida[‡]

Institute for Theoretical Physics, Kanazawa University,

Kanazawa 920-1192, Japan

Abstract

The radiative seesaw model with an inert doublet has been shown to be attractive from a viewpoint of both neutrino masses and cold dark matter. However, if we apply this model to the explanation of the positron excess in the cosmic ray observed by PAMELA, a huge boost factor is required although it can be automatically explained that no anti-proton excess has been observed there. We consider an extension of the model to enhance the thermally averaged annihilation cross section without changing the features of the model favored by both the neutrino oscillation and the relic abundance of dark matter. It is shown that the data of PAMELA and Fermi-LAT can be well explained in this extended model. Constraints from gamma ray observations are also discussed.

[*]e-mail: suematsu@hep.s.kanazawa-u.ac.jp

[†]e-mail: t-toma@hep.s.kanazawa-u.ac.jp

[‡]e-mail: yoshida@hep.s.kanazawa-u.ac.jp

1   Introduction

The existence of dark matter (DM) now gives us a clear motivation to investigate physics beyond the standard model (SM). Although we know its relic abundance in the present universe[1], its nature is not clarified except that DM should be cold. However, recent observational data on cosmic rays may give us interesting information on its mass and interactions. PAMELA has reported positron excess in the cosmic ray at the 6 - 100 GeV range in comparison with the expected background [2]. However, it has observed no anti-proton excess. The preliminary report of Fermi-LAT also suggests that the total flux of positrons and electrons is larger than the expected background at regions of 60 - 1000 GeV [3], although any bump shown in the ATIC result [4] is not found in that flux. If we consider these results are caused by the decay or the annihilation of DM but not by astrophysical origins, they are expected to give us crucial information on the nature of DM. However, it has been pointed out that there is a difficult problem if we try to understand these results on the basis of DM physics.

In case of the DM decay, DM life time should be extremely long such as $O(10^{26})$ sec in order to explain the PAMELA positron excess [5, 6]. It is not so easy to answer how such a long lifetime can be naturally realized in the ordinary models for elementary particles, although there are several proposals to solve this problem. In case of the DM annihilation, its relic abundance requires the thermally averaged annihilation cross section $\langle \sigma v \rangle$ to be $O(10^{-26})$ cm^3/sec at its freeze-out period where the typical DM velocity $v_{\rm DM}$ satisfies $v_{\rm DM}/c \sim 0.2$. On the other hand, the positron excess found in the PAMELA experiment requires $\langle \sigma v \rangle$ to be $O(10^{-23})$ cm^3/sec for the DM in our Galaxy where $v_{\rm DM}/c \sim 10^{-3}$ is expected for the averaged DM velocity. This means that there should be some large enhancement introduced as a boost factor usually, which may be caused by particle physics, or astrophysics, or both of them. There have been several analyses on this point [7, 8]. In this paper, we focus our attention on the particle physics side and study a way to overcome this difficulty in a model for both neutrino mass and DM.

The radiative seesaw model proposed in [9] gives an attractive scenario for the neutrino mass and mixing. They are explained by new physics at TeV scales in this model. The model includes DM candidates whose stability is guaranteed by a discrete symmetry. It forbids bare Dirac mass terms of neutrinos and then is related to the smallness of neutrino masses. The model has been studied from various points of view [10, 11, 12, 13].

However, if we apply this model to explain the PAMELA data by the DM annihilation, we confront the boost factor problem, unfortunately. In this model the annihilation cross section has a dominant contribution from its p-wave part. Since the p-wave contribution becomes smaller for smaller DM relative velocity v, the situation is much worse than the s-wave case. In fact, this requires a huge boost factor of $O(10^6)$ to explain the PAMELA data on the basis of this model unless there are some additional astrophysical effects [12, 13]. On the other hand, we should also remind the reader that the model has an interesting feature favored by the PAMELA data, that is, the DM can annihilate only to leptons. Moreover, if we impose constraints on the model from the lepton flavor violating processes like $\mu \to e\gamma$, $e^\pm$ should not be yielded as the primary final states of the annihilation. Positrons originated from this DM annihilation are generated through the decay of μ^+ and $\tau^\pm$ [13]. Model independent analyses suggest that this feature is again favored by both data of PAMELA and Fermi-LAT [8]. Thus, it is an interesting subject for this model to find some solutions for this boost factor problem by extending the model without disturbing these nice features of the model.[d]

In this paper we propose a simple extension of the model, which makes the Breit-Wigner enhancement of thermally averaged annihilation cross section possible. In that model we show that both data of PAMELA and Fermi-LAT can be well explained without assuming an unknown huge boost factor as long as the mass of a scalar field is finely tuned. The enhanced annihilation cross section may also predict the large flux of gamma ray which is associated with the DM annihilation. We discuss the consistency with the data for the diffuse gamma ray from observations in the EGRET, HESS and Fermi-LAT experiments.

The following parts of the paper are organized as follows. In section 2 we fix the radiative seesaw model and discuss how all the neutrino oscillation data, lepton flavor violating processes and the DM relic abundance can be consistently explained. After that we extend the model to enhance the DM annihilation cross section in the present Galaxy. In section 3 we address the features required for the explanation of the data of PAMELA and Fermi-LAT. We also discuss the consistency between the diffuse gamma ray flux expected in the model and the present experimental data. We summarize the

---

[d]One solution has been proposed by considering the decaying DM in a supersymmetric extension of the model [6].

paper in section 4.

2 Breit-Wigner enhancement

2.1 A radiative seesaw model

The radiative seesaw model considered here is an extension of the SM with an inert doublet η (an additional $SU(2)_L$ doublet scalar with $\langle\eta\rangle = 0$) and three gauge singlet right-handed fermions N_k ($k = 1, 2, 3$) [9]. In order to forbid tree-level Dirac masses for neutrinos, we impose Z_2 symmetry on the model. An odd charge of this Z_2 symmetry is assigned to all of these new fields, although an even charge is assigned to all of the SM contents. Both interaction Lagrangian $\mathcal{L}_N$ relevant to N_k and scalar potential V invariant under the imposed symmetry are written as

$$
\begin{aligned}
\mathcal{L}_N &= -\left(M_k \overline{N_k^c} P_R N_k + M_k \overline{N_k} P_L N_k^c\right) - (h_{\alpha k}\overline{\ell_\alpha}\eta P_R N_k + \text{h.c.}), \\
V &= m_\phi^2 \phi^\dagger\phi + m_\eta^2 \eta^\dagger\eta + \lambda_1(\phi^\dagger\phi)^2 + \lambda_2(\eta^\dagger\eta)^2 + \lambda_3(\phi^\dagger\phi)(\eta^\dagger\eta) + \lambda_4(\phi^\dagger\eta)(\eta^\dagger\phi) \\
&+ \frac{\lambda_5}{2}\left[(\phi^\dagger\eta)^2 + \text{h.c.}\right],
\end{aligned}
\tag{1}
$$

where ℓ_α and ϕ stand for a left-handed lepton doublet and an ordinary Higgs doublet scalar, respectively. Coupling constants and masses of singlet fermions are assumed to be real, for simplicity. $\mathcal{L}_N$ is assumed to be written by using the basis in which a charged lepton mass matrix is diagonal.

The model has several interesting features [10, 11, 12, 13]. First, neutrino masses are generated through one-loop diagrams as

$$
\begin{aligned}
\mathcal{M}_{\alpha\beta} &= \sum_k \Lambda_k h_{\alpha k} h_{\beta k}, \\
\Lambda_k &= \frac{\lambda_5\langle\phi\rangle^2}{8\pi^2 M_k} I\left(\frac{M_k^2}{M_\eta^2}\right), \qquad I(x) = \frac{x}{1-x}\left(1 + \frac{x \ln x}{1-x}\right),
\end{aligned}
\tag{2}
$$

where $M_\eta^2 = m_\eta^2 + (\lambda_3 + \lambda_4)\langle\phi\rangle^2$. This neutrino mass matrix can explain the neutrino oscillation data well as long as we set appropriate values for the parameters λ_5, $h_{\alpha k}$, M_k and M_η. We note that λ_5 should be very small to generate desired neutrino masses. However, this tuning is not so bad nature since it can be controlled by a global symmetry

which appears if we make λ_5 zero.[e] Second, the lightest one of N_k can be DM since its stability is guaranteed by the Z_2 symmetry. Its relic density can be adjusted to the one required by WMAP for the same parameters used for the explanation of the neutrino oscillation data. Third, these are also consistent with the constraints imposed by the lepton flavor violating processes such as $\mu \to e\gamma$ and $\tau \to \mu\gamma$, if neutrino Yukawa couplings $h_{\alpha k}$ have certain flavor structure.[f]

In order to show these aspects concretely, we consider an example of such flavor structure for neutrino Yukawa couplings as

$$h_{ei} = 0, \quad h_{\mu i} = h_{\tau i} \ (i = 1, 2); \quad h_{e3} = -h_{\tau 3}, \qquad h_{\mu 3} = -h_{\tau 3}. \tag{3}$$

In this case the neutrino mass matrix can be written as

$$\mathcal{M} = \begin{pmatrix} 0 & 0 & 0 \\ 0 & 1 & 1 \\ 0 & 1 & 1 \end{pmatrix} (h_{\tau 1}^2 \Lambda_1 + h_{\tau 2}^2 \Lambda_2) + \begin{pmatrix} 1 & 1 & -1 \\ 1 & 1 & -1 \\ -1 & -1 & 1 \end{pmatrix} h_{\tau 3}^2 \Lambda_3, \tag{4}$$

and the tri-bimaximal neutrino mixing is automatically realized for the neutrino mass matrix (2) [13]. Moreover, only two mass eigenvalues take nonzero values. Thus, the neutrino oscillation data can be consistently explained as long as the following conditions are satisfied:

$$h_{\tau 1}^2 \Lambda_1 + h_{\tau 2}^2 \Lambda_2 \simeq 2.5 \times 10^{-2} \text{ eV}, \qquad h_{\tau 3}^2 \Lambda_3 \simeq 2.9 \times 10^{-3} \text{ eV}. \tag{5}$$

These come from the required values for Δm_{atm}^2 and $\Delta m_{\text{solar}}^2$, respectively. We need to consider the constraints from both the lepton flavor violating processes and the DM relic abundance under these conditions. The relation of Yukawa couplings $h_{\alpha k}$ to other parameters λ_5, M_k and M_η is also determined through these constraints. When we apply eq. (5) to the analysis, it may be useful to note that these give the constraints on the value of $h_{\tau k}^2 \lambda_5$ for the fixed M_k and M_η. In particular, Λ_k is proportional to $h_{\tau k}^2 \lambda_5 M_k / M_\eta^2$ for $M_k \ll M_\eta$ since $I(x) \simeq x$ for $x \ll 1$. Since $h_{\tau k}$ tends to be smaller for larger values

---

[e]This problem may also be solved by making the λ_5 term as an effective one through the extension of the model with a U(1) gauge symmetry [11].

[f]There is a severe tension between the relic abundance and the lepton flavor violation generally [10, 11]. If we make neutrino Yukawa couplings small enough to suppress the lepton flavor violation, the DM relic abundance becomes too large.
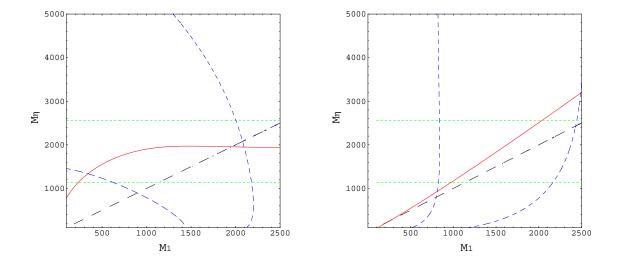
Fig. 1 Contours for the branching ratio of the lepton flavor violating processes and the DM relic abundance in the (M_1, M_η) plane. The left and right panel corresponds to case (i) and (ii) defined in the text, respectively. Green dotted lines represent the contours for $Br(\mu \to e\gamma) \times 10^{11} = 1.2, 0.72$ in M_η decreasing order. Blue dashed lines represent the ones for $Br(\tau \to \mu\gamma) \times 10^8 = 0.68, 0.068$ in M_1 increasing order. The red solid line in the $M_1 < M_\eta$ region corresponds to the contour for the N_1 relic abundance $\Omega_{N_1} h^2 = 0.11$ required by the WMAP. The black long dashed line represents a line for $M_1 = M_\eta$.

of λ_5, λ_5 is expected to have values in restricted regions by taking account of the DM relic abundance condition as seen later. We will assume $M_1 < M_\eta$ throughout the present analysis.

The branching ratio of the lepton flavor violating process $\ell_\alpha \to \ell_\beta\gamma$ is written as [14]

$$Br(\ell_\alpha^- \to \ell_\beta^-\gamma) = \frac{3\alpha}{64\pi(G_F M_\eta^2)^2} \left[\sum_{k=1}^{3} h_{\alpha k} h_{\beta k} F_2\left(\frac{M_k^2}{M_\eta^2}\right)\right]^2 Br(\ell_\alpha^- \to \ell_\beta^- \bar{\nu}_\beta \nu_\alpha),$$

$$F_2(x) = \frac{1 - 6x + 3x^2 + 2x^3 - 6x^2 \ln x}{6(1-x)^4}. \tag{6}$$

If we use the condition (3), we find that

$$Br(\mu \to e\gamma) \simeq \frac{3\alpha}{64\pi(G_F M_\eta^2)^2} \left[h_{\tau 3}^2 F_2\left(\frac{M_3^2}{M_\eta^2}\right)\right]^2,$$

$$Br(\tau \to \mu\gamma) \simeq \frac{0.51\alpha}{64\pi(G_F M_\eta^2)^2} \left[h_{\tau 1}^2 F_2\left(\frac{M_1^2}{M_\eta^2}\right) + h_{\tau 2}^2 F_2\left(\frac{M_2^2}{M_\eta^2}\right) - h_{\tau 3}^2 F_2\left(\frac{M_3^2}{M_\eta^2}\right)\right]^2. \tag{7}$$

By using these formulas and eqs. (5), the expected values for the branching ratio of $\mu \to e\gamma$ and $\tau \to \mu\gamma$ can be plotted in the (M_1, M_η) plane by fixing parameters $h_{\tau 1}$, λ_5, M_2,
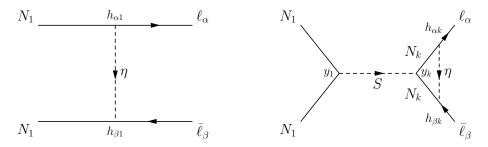
Fig. 2 Diagrams contributing to the N_1 annihilation.

and M_3. Here we consider two cases: (i) $M_1 < M_2 < M_3$ and (ii) $M_1 \simeq M_2 < M_3$. In both cases λ_5 and M_3 are treated as free parameters. Since $h_{\tau 1}$ and M_2 are determined by other parameters in case (ii), this case is much constrained and predictive compared with case (i).

In Fig. 1 we show the contours of these branching ratios for typical parameters. Here we use $\lambda_5 = 6.0 \times 10^{-11}$ and $M_3 = 4.8$ TeV. In case (i), we fix the remaining parameters as $h_{\tau 1} = 1.5$ and $M_2 = 2.8$ TeV. Green dotted lines and blue dashed lines represent the contours of $Br(\mu \to e\gamma)$ and $Br(\tau \to \mu\gamma)$, respectively. The former one is independent of M_1 in both cases (i) and (ii). This is clear from the expression in eq. (7). Moreover, this branching ratio becomes sufficiently small by making M_3 large enough. It should be noted that $F_2(M_3^2/M_\eta^2)$ becomes smaller for larger M_3 although larger M_3 makes $h_{\tau 3}$ larger through eq.(5). On the other hand, $Br(\tau \to \mu\gamma)$ shows different behavior in each case. It is independent of M_η in case (ii) for the $M_\eta > M_1$ region. This is expected from the feature of Λ_k which is previously remarked on eqs. (5) and (7). In case (i), $Br(\tau \to \mu\gamma)$ is not largely affected by changing M_2 and M_3 as long as $h_{\tau 1} > h_{\tau 2}$ is satisfied, which is favored by the DM relic abundance as seen later. The present experimental bounds [17] are found to be satisfied in the wide range of parameter space shown in this figure. The model can be easily consistent with both the neutrino oscillation data and the bounds from the lepton flavor violating processes as long as parameters are suitably selected.

Next we discuss the nature of DM in this model. Since N_1 is assumed to be DM, the condition (3) suggests that charged final states yielded in the DM annihilation consist of $\mu^\pm$ or $\tau^\pm$ only. Positron and electron are only induced through the decay of these particles. It should be reminded again that this nature of DM is favored by the anomaly suggested by PAMELA and Fermi-LAT. The DM relic abundance is determined through the N_1 annihilation, which occurs through the t-channel η exchange diagram shown in

Fig. 2. The dominant contribution comes from the p-wave process. Thus, the annihilation cross section averaged by the spin of initial states is expressed as[g]

$$\sigma_1 v = \frac{1}{3\pi} \frac{M_1^2 (M_1^4 + M_\eta^4)}{(M_1^2 + M_\eta^2)^4} h_{\tau i_1}^2 h_{\tau i_2}^2 v^2, \tag{8}$$

where we use eq. (3) to derive this formula. In case (i), $i_1 = i_2 = 1$ should be understood and then $\sigma_1 v \propto h_{\tau 1}^4$. On the other hand, if the masses of N_1 and N_2 are almost degenerate as in case (ii), coannihilation plays a role and then the contribution of $i_{1,2} = 1$ and 2 should be summed up. As its result, we have $\sigma_1 v \propto (h_{\tau 1}^2 + h_{\tau 2}^2)^2$ [13].

In order to estimate the freeze-out temperature T_f of N_1 including the coannihilation case, we follow the procedure given in [15, 16]. We define $\sigma_{\rm eff}$ and $g_{\rm eff}$ as

$$
\begin{aligned}
\sigma_{\rm eff} &= \frac{g_{N_1}^2}{g_{\rm eff}^2} \sigma_{N_1 N_1} + 2 \frac{g_{N_1} g_{N_2}}{g_{\rm eff}^2} \sigma_{N_1 N_2} (1+\delta)^{3/2} e^{-x\delta} + \frac{g_{N_2}^2}{g_{\rm eff}^2} \sigma_{N_2 N_2} (1+\delta)^3 e^{-2x\delta}, \\
g_{\rm eff} &= g_{N_1} + g_{N_2} (1+\delta)^{3/2} e^{-x\delta}, \tag{9}
\end{aligned}
$$

where $x = M_1/T$ and $m_{\rm pl} = 1.22 \times 10^{19}$ GeV. Internal degrees of freedom of N_i are described by g_{N_i} and δ is defined by $\delta \equiv (M_2 - M_1)/M_1$. If we define $a_{\rm eff}$ and $b_{\rm eff}$ by $\sigma_{\rm eff} v = a_{\rm eff} + b_{\rm eff} v^2$, the thermally averaged cross section can be written as $\langle \sigma_{\rm eff} v \rangle = a_{\rm eff} + 6 b_{\rm eff}/x$. In case (i), $\sigma_{\rm eff}$ and $g_{\rm eff}$ are dominated by the first term since $\delta > 0.2$ [16]. On the other hand, $\delta \ll 1$ is assumed in case (ii). Thus, the second and third terms can bring the important contribution. Using these, the relic abundance of N_1 can be estimated through the formulas

$$\Omega_{N_1} h^2 = \frac{1.07 \times 10^9 x_f}{g_*^{1/2} m_{\rm pl} ({\rm GeV})(a_{\rm eff} + 3 b_{\rm eff}/x_f)}, \quad x_f = \ln \frac{0.038 g_{\rm eff} m_{\rm pl} M_1 (a_{\rm eff} + 6 b_{\rm eff}/x_f)}{g_*^{1/2} x_f^{1/2}}, \tag{10}$$

where g_* is the relativistic degrees of freedom at the freeze-out temperature T_f of N_1.

By using these formulas and the conditions in eq. (5), we can plot the contour $\Omega_{N_1} h^2 = 0.11$ required by WMAP in the (M_1, M_η) plane. In Fig. 1, it is drawn by a red solid line in each case (i) and (ii) for the same values of parameters used in the estimation of $Br(\ell_\alpha \to \ell_\beta \gamma)$. The result in each case depends on $h_{\tau 1}^2$ and $h_{\tau 1}^2 + h_{\tau 2}^2$, respectively. Since it also depends on λ_5 through the relations (5) as noted before, the required $\Omega_{N_1} h^2$ can be obtained only for rather restricted values of λ_5. In Fig. 1, the points on the red solid line

---

[g] We need to remind that final states also include neutrino pairs other than the charged lepton pairs for the relic abundance estimation.

in the region satisfying both $Br(\mu \to e\gamma) < 1.2 \times 10^{-11}$ and $M_1 < M_\eta$ give the parameters consistent with all of the neutrino oscillation data and constraints from the lepton flavor violating process and the DM relic abundance. Thus, we find that the present model can give a very simple and consistent framework for the known experimental results.

The values of relevant Yukawa couplings are determined for each point on the $\Omega_{N_1} h^2 = 0.11$ line. In Fig. 1, we have, for example,

$$
\begin{aligned}
&\text{(i)} \quad h_{\tau 2} = 1.40, \quad h_{\tau 3} = 0.66 && \text{at } (M_1, M_\eta) = (1600, 1950), \\
&\text{(ii)} \quad \sqrt{h_{\tau 1}^2 + h_{\tau 2}^2} = 2.14, \quad h_{\tau 3} = 0.66 && \text{at } (M_1, M_\eta) = (1600, 1950).
\end{aligned}
\tag{11}
$$

If we make λ_5 larger for the fixed M_1, larger values for M_η and $h_{\tau 1}$ are required as expected from eq. (8). On the other hand, λ_5 is bounded from below by the condition $M_\eta > M_1$. Thus, neutrino Yukawa couplings are required to take rather large values by the DM relic abundance. This suggests that the model may be inconsistent due to these large Yukawa couplings, which may make the scalar potential unstable at the energy regions above a certain cut off scale μ. If this cut-off scale does not satisfy $\mu > M_3$, the present scenario can not work. Since larger M_3 is favored from the $\mu \to e\gamma$ constraint, we can not make M_3 smaller enough for this instability problem. Thus, this imposes nontrivial constraint on the model. Since λ_2 is most affected by the large neutrino Yukawa couplings $h_{\tau k}$, the cut-off scale μ is determined as the scale where λ_2 becomes negative.

We examine this point by studying the behavior of couplings included in $\mathcal{L}_N$ and V to fix μ using renormalization group equations (RGEs) for them. These RGEs are given in Appendix A. Numerical analysis is practiced for the parameters given in (11) assuming the $O(1)$ values for the couplings λ_i. This analysis shows that $\mu = O(10)$ TeV and then $\mu > M_3$ is possible for these values of couplings at low energy regions. The scenario seems to be consistent with the potential instability. However, it is difficult to make μ much larger than M_3. If N_k and η are supposed to be suitable representations of some hidden non-Abelian gauge symmetry under which all the SM contents are singlet, some improvement may be expected for this situation. As such an example, we may consider SU(2) symmetry and both N_k and η are doublet of that gauge symmetry. In such an extension, $\mathcal{L}_N$ and V are invariant and no anomaly problem occurs within these field contents. The RGE study of this case shows that μ can be somewhat large. However, it is difficult to make μ larger than M_3 by more than one order since the running region of the relevant RGEs is too short. Thus, although the model can escape the instability

of the potential, we need to consider some fundamental model at the scale not far from M_3. Since this argument on the potential stability suggests that smaller neutrino Yukawa couplings are favored, smaller values of M_1 and λ_5 are also favored from the N_1 relic abundance. On the other hand, as discussed in the next part, only a limited value of M_1 seems to be favored from the explanation of the charged cosmic ray anomaly. This suggests that λ_5 is also required to take its value in the strictly restricted region.

It is worthy to note that we can predict the expected values for the branching ratio of $\mu \to e\gamma$ and $\tau \to \mu\gamma$ in this model from Fig. 1, if we can fix the value of M_1 further by using other experimental data. Observational data on the cosmic rays from PAMELA and Fermi-LAT experiments may be used for such a purpose. However, if we suppose the PAMELA anomaly as a consequence of the annihilation of this DM, we confront difficulty. The annihilation cross section is found to be too small to explain the PAMELA positron excess for the typical relative velocity of DM in the present Galaxy as mentioned before. In the next part we propose an extension of the model to overcome this fault.

2.2   Extension of the model

We consider the introduction of a new interaction which brings a large contribution to the N_1 annihilation only at the present Galaxy and also does not modify the previously discussed favorable features of the model. For that purpose, we add a complex singlet scalar S with even parity of the Z_2 symmetry.[h] This singlet scalar is assumed to have mass M_S and couplings with other fields through the Lagrangian through the interaction Lagrangian

$$\mathcal{L}'_N = -y_k S \overline{N_k^c} P_R N_k - y_k^* S^* \overline{N_k} P_L N_k^c - M_S^2 |S|^2 - \kappa |S|^4 - \left(\kappa_\phi \phi^\dagger \phi + \kappa_\eta \eta^\dagger \eta\right) |S|^2. \quad (12)$$

Here we note that this is not the most general Lagrangian under the imposed symmetry. However, although interaction terms like $\phi^\dagger \phi S$ and $\eta^\dagger \eta S$ which are not forbidden by the symmetry can be radiatively induced, they are largely suppressed as long as S is assumed to have no vacuum expectation value.[i] In that case, S dominantly decays to N_k with the mass $M_k < M_S/2$. In this extended model, we find that there appears a new one-loop contribution to the annihilation of N_1 as shown in Fig. 2.

---

[h]The extension of the model by a singlet scalar field has been considered in other context in [18].

[i]This assumption is justified only if the tadpole diagram for S generated through the N_k loop is cancelled by cS which can be introduced in Lagrangian. We consider such a situation here.

This new contribution to the N_1 annihilation cross section can be estimated as

$$(\sigma_2 v)_{\alpha\beta} = \frac{1}{\pi} \frac{M_1^2}{M_\eta^4} \frac{m_\alpha^2 + m_\beta^2}{(s - M_S^2)^2 + M_S^2 \Gamma_S^2} \left(\sum_{k=1}^{3} \frac{|y_1 y_k| h_{\alpha k} h_{\beta k} M_k}{(4\pi)^2 D_k} \right)^2, \tag{13}$$

where the spin of initial states is averaged. We fix the final states to be charged leptons with masses $m_{\alpha,\beta}$ in this expression. This annihilation cross section is dominated by the contribution from the exchange of a pseudoscalar component. To obtain the total annihilation cross section, α and β should be summed up for all possible final states as $\sigma_2 v = \sum_{\alpha\beta} (\sigma_2 v)_{\alpha\beta}$. The definition of s, Γ_S and $1/D_k$ are given by

$$s = E_{\text{cm}}^2 \simeq 4M_1^2 \left(1 + \frac{v^2}{4} \right),$$

$$\Gamma_S = \frac{|y_1|^2}{8\pi} M_S \sqrt{1 - 4\frac{M_1^2}{M_S^2}} \left(1 - 2\frac{M_1^2}{M_S^2} \right),$$

$$\frac{1}{D_k} = \int_0^1 dz \, \frac{1}{1 - r_k + 4r_1 z} \log \left| \frac{1 - (1 - r_k)z}{r_k - 4r_1 z(1 - z)} \right|, \tag{14}$$

where $r_k = M_k^2/M_\eta^2$ and S is supposed to decay to the N_1 pair only. This type of annihilation cross section has been suggested to be enhanced sufficiently for the explanation of the PAMELA data [19]. In fact, if the thermal average of $(\sigma v)_{\alpha\beta}$ is estimated naively by replacing v^2 with a thermally averaged value $\frac{6}{x}$ in eq. (13), the annihilation cross section shows the Breit-Wigner resonance at $x_r = \frac{3}{2\Delta}$ through the factor $[(\Delta - \frac{3}{2x})^2 + \gamma_S^2]^{-1}$, where we use the definition $\Delta \equiv 1 - \frac{4M_1^2}{M_S^2}$ and $\gamma_S \simeq \frac{1}{16\pi} |y_1|^2 \Delta^{1/2}$. However, such a naive treatment has been shown to be unreliable near a resonance point [16, 20]. The enhancement of the annihilation cross section is overestimated in such a naive method. To obtain the correct enhancement, we need to calculate the thermal average

$$\langle \sigma_2 v \rangle_{\alpha\beta} = \frac{x^{3/2}}{2\pi^{1/2}} \int_0^\infty dv \, v^2 (\sigma_2 v)_{\alpha\beta} e^{-xv^2/4}. \tag{15}$$

Although this formula is derived in the center of mass system, the result is expected to be reliable since N_1 is sufficiently non-relativistic in the present case [16, 20].

In order to find the qualitative feature, it is useful to approximate this integral by expanding v as $v = v_r + \nu$ around the peak value $v_r = 2\Delta^{1/2}$. Then, eqs. (13) and (15)

give

$$\langle\sigma_2 v\rangle_{\alpha\beta} \simeq \frac{x^{3/2}}{2\pi^{3/2}} \frac{(m_\alpha^2 + m_\beta^2)M_1^2}{M_\eta^4 M_S^4} \left(\sum_{k=1}^{3} \frac{|y_1 y_k| h_{\alpha k} h_{\beta k} M_k}{(4\pi)^2 D_k}\right)^2 e^{-x\Delta} \int_{-\nu_0}^{\nu_0} d\nu \frac{1}{\nu^2 \Delta + \gamma_S^2}$$

$$\simeq \frac{2\pi^{1/2}}{(4\pi)^4} \frac{(m_\alpha^2 + m_\beta^2)}{M_\eta^4} \left(\sum_{k=1}^{3} \frac{|y_k| h_{\alpha k} h_{\beta k} M_k}{D_k M_1}\right)^2 x^{3/2} e^{-x\Delta}, \tag{16}$$

where $\nu_0 \ll v_r$ and $16\pi\nu_0 \gg |y_1|^2$ are assumed. Using this result, we roughly estimate this resonance effect on the annihilation cross section caused by the diagram which has N_k as the internal fermions and $\tau^\pm$ in final states. For that purpose, we take $x_r \simeq 10^6$ which is just coincident with the typical relative velocity $2 \times 10^{-3}c$ of this DM in the present Galaxy. The annihilation cross section at x_r is found to satisfy the relation [j]

$$\frac{\langle\sigma_2 v\rangle}{10^6 \langle\sigma_1 v\rangle} \sim \left(\frac{M_k}{M_1 D_k}\right)^2 \left(\frac{h_{\tau k}}{\tilde{h}}\right)^4 |y_k|^2, \tag{17}$$

where $\tilde{h} = h_{\tau 1}$ and $\sqrt{h_{\tau 1}^2 + h_{\tau 2}^2}$ for the annihilation and the coannihilation, respectively. The first two factors relevant to the masses and the neutrino Yukawa couplings of N_k are fixed by the conditions imposed by the neutrino oscillation and the N_1 relic abundance. The first factor is estimated to be $O(1)$ and decreases for larger M_k. The second factor is considered to be less than 1 except for the coannihilation case where it can be almost 1. Since $|y_1|$ is assumed small in the above discussion, we find that the desirable enhancement can be expected from the N_2 contribution with $|y_2| = O(1)$. These show that the sufficient enhancement factor to explain the PAMELA data can be obtained through the Breit-Wigner resonance at least in the coannihilation case.

To obtain much quantitative estimation we calculate the thermally averaged annihilation cross section by integrating eq. (15) numerically. The result for $\langle\sigma v\rangle = \langle\sigma_1 v\rangle + \langle\sigma_2 v\rangle$ is plotted as a function of x in Fig. 3. In this calculation we use the parameters given in Table 1, which can realize a point on the red line in Fig. 1. They satisfy all the neutrino oscillation data, the DM relic abundance required by WMAP and the constraints from the lepton flavor violating processes. Since the interference terms between tree diagrams and one-loop diagrams can be neglected in both regions $v_f/c \sim 0.2$ and $v_r/c \lesssim 10^{-3}$, the figure shows that we can safely use $\langle\sigma_1 v\rangle$ and $\langle\sigma_2 v\rangle$ in each region, respectively. In this

---

[j]Here the annihilation cross section $\langle\sigma_2 v\rangle$ is defined as $\langle\sigma_2 v\rangle = 4\langle\sigma_2 v\rangle_{\mu^\pm \tau^\mp}$ by taking account of all possible modes. See eqs.(22) and (23) also.
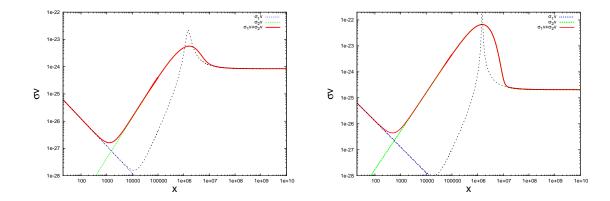
Fig. 3 The N_1 annihilation cross section as a function of $x(\equiv \frac{6}{\langle v^2 \rangle})$. The left and right panel corresponds to the case (i) and (ii), respectively. Parameters in the annihilation cross section are fixed to the ones shown in Table 1. The thin black dashed line shows the result for $\langle \sigma v \rangle$ obtained by the naive method.

figure the result obtained by the naive method is also plotted by a thin black dashed line. It shows that the enhancement effect is overestimated and the annihilation cross section is misled to be large enough for the explanation of the PAMELA data in both cases (i) and (ii). However, the correct calculation shows that the enhancement can not be large enough for reasonable values of $|y_k|$ in the annihilation case (i). On the other hand, in the coannihilation case (ii), we find that the Breit-Wigner resonance can make the annihilation cross section have a desirable value 10^{-23} cm^3/sec around $v \simeq v_r$ as long as Δ and $|y_k|$ have suitable values. Here we should note that this value of Δ requires M_S to be finely tuned to M_1 at the level of $O(10^{-6})$. We also comment on the instability of this solution induced by radiative corrections. A dominant correction to the singlet scalar mass M_S at the one-loop level is roughly estimated as $\delta M_S^2 \simeq \frac{y_2^2}{(4\pi)^2}\mu^2$ where μ is the cut-off scale of the model. Since μ is rather small and $\mu = O(10)$ TeV as discussed before, we find that

	M_1	M_η	$h_{\tau 1}$	$h_{\tau 2}$	$h_{\tau 3}$	Δ	$|y_1|$	$|y_2|$	$|y_3|$
(i)	1.6	1.95	1.5	1.4	0.66	10^{-6}	0.1	2.5	0.01
(ii)	1.6	1.95	0.1	2.14	0.66	10^{-6}	0.015	1.715	0.01

Table 1 Parameter sets used to draw the annihilation cross section behavior in Fig. 2 and also to obtain the positron spectrum in Fig. 4. Masses are given in TeV unit. We set $\lambda_5 = 6.0 \times 10^{-11}$ and $M_3 = 4.8$ TeV for each case.

δM_S^2 is the same order value as the required M_S. This means that we need the fine tuning of $O(10^{-6})$ to keep the stability of this solution from the radiative corrections. The large value of y_2 may require the fine tuning up to the eight-loop order. Unfortunately, the model does not have any physical background to guarantee the required mass relation. It remains as a difficult problem how to realize this finely tuned situation from the basic model at high energy regions.

It is worthwhile to stress that these values of Δ and $|y_k|$ can be fixed without contradicting the required DM relic abundance which is determined by the annihilation process described by eq. (8). The reason is that different parameters are relevant to determine the DM relic abundance and the positron flux, respectively.[k] Although the former is determined by M_1, M_η and $h_{\tau k}$, the latter is mainly determined by $|y_k|$ and Δ. We note that the parameters relevant to the enhancement of the annihilation cross section required for the explanation of PAMELA and FERMI-LAT are confined to y_1, y_2 and M_S, although a lot of free parameters seems to be introduced in eq. (12). It seems to be interesting that these limited parameters can also allow the model to satisfy the reionization constraints as discussed below.[l]

It is also useful to note that it is crucial that the annihilation occurs through a one-loop diagram in the present enhancement mechanism. This is clear from the fact that the enhancement is caused by the existence of N_k, which satisfies $|y_k| \gg |y_1|$ and $h_{\tau k} \sim \tilde{h}$.[m] Although these conditions can be satisfied in the coannihilation case, in the annihilation case larger $h_{\tau 2}$ requires relatively smaller $h_{\tau 1}$ as seen from eq.(5). However, small $h_{\tau 1}$ contradicts the condition imposed by the N_1 relic abundance. Thus, only the coannihilation case can realize $\langle \sigma_2 v \rangle \sim 10^{-23}$ cm^3/sec for each M_1 by adjusting the values of $|y_k|$ and $|y_1|$ without affecting the N_1 relic abundance.

---

[k] It is useful to note that the similar aspect is found in the case of Sommerfeld enhancements. If only a single annihilation channel is assumed, Sommerfeld enhancements cause a discrepancy between the relic density and the excesses of positron flux [21]. The present model escapes this by considering two processes given in Fig. 2.

[l] The relevant parameters contained in eq. (1) have already been fixed to explain the neutrino oscillation data (two squared mass differences and three mixing angle), the DM relic abundance Ωh^2 and lepton flavor violating processes. Taking account of the supposed flavor structure, they are $M_{1,3}, M_\eta, \lambda_5$ and $h_{\tau_1}, h_{\tau_2}, h_{\tau_3}$ in the coannihilation case.

[m] It is worthy to note that numerical calculation shows that $\langle \sigma_2 v \rangle$ has the largest value for $y_1 \simeq 0.1$ and 0.01 at $x = x_r$ in the case (i) and (ii) respectively. It slowly decreases for larger $|y_1|$.

One may worry about the potential instability caused by the large value of $|y_2|$ shown in Table 1. In fact, the coupling constants κ and κ_η can become negative at a scale smaller than M_3 as long as η and N_k are singlets of the hidden gauge symmetry. However, if they are doublets of the hidden SU(2), the coupling constant y_k in $\langle \sigma_2 v \rangle$ is replaced by $2y_k$ because of the gauge freedom in the one-loop diagram. This shows that a rather small value $y_2 \simeq 0.86$ is needed to realize the required enhancement of $\langle \sigma_2 v \rangle$. We can numerically check that this value of y_2 improves the above mentioned potential instability problem to make the extended model consistent. In this case the cut-off scale of the model is still determined by the behavior of λ_2.

Finally we note the values of the annihilation cross section at the recombination period $z \sim 1000$, which corresponds to the DM relative velocity $v/c \sim 10^{-8}$. The DM annihilation in the period after recombination to structure formation ($z \gtrsim 6$) causes the deposition of energy in the inter galactic medium, which brings an additional origin for the reionization and heating of the intergalactic gas. This additional effect is constrained from the observed optical depth of the universe and the measured temperature of the intergalactic gas. In particular, the optical depth bound brings severe constraint on the high mass DM as the present model since it can produce too many free electrons. If we follow the analysis for these constraints given in [22], the annihilation cross section should satisfy $\langle \sigma_2 v \rangle \lesssim 10^{-24}$ cm^3/sec for the DM with the mass 1600 GeV. In Fig. 3, we find that this constraint is satisfied at $v/c \lesssim 10^{-5}$. It corresponds to the environments in which most of the annihilation contribution to the relevant signal is considered to take place. Here it is useful to note that $\langle \sigma_2 v \rangle$ does not decrease to 10^{-24} cm^3/sec even for much smaller relative velocity $v < v_r$ and keep larger values than that if $|y_1| \lesssim 0.05$ is not satisfied. Thus, the reionization constraint rules out these cases. As long as this condition is satisfied, the present DM scenario can be consistent with the constraint caused by the effect on the reionization due to their annihilation.[n] In the next section we apply this extended model to the explanation of the anomaly suggested in PAMELA and Fermi-LAT experiments.

---

[n] Since the Sommerfeld enhancement shows an inverse proportionality to the relative velocity of the two DM fields, it could cause different effects on the reionization from this model.

3 Positron flux and gamma ray constraints

We estimate the positron flux yielded by the N_1 annihilation following the method used in [23, 24] and compare it with the data obtained in the PAMELA and Fermi-LAT experiments. The positron flux in the cosmic ray at the Earth is expressed as $\Phi_{e+}(E) = v_{e+} f(E)/4\pi$ $(\text{GeV} \cdot \text{cm}^2 \cdot \text{str} \cdot \text{sec})^{-1}$ where v_{e+} is positron velocity. $f(E)$ is the positron number density per unit energy at the Earth, which can be determined by solving the diffusion equation for $f(E)$. Using the approximated solution for $f(E)$, the positron flux Φ_{e+} expected from the N_1 annihilation is estimated as

$$\Phi_{e+}(E) = \frac{v_{e+}}{8\pi E^2/(\text{GeV } \tau_E)} \left(\frac{\rho_{N_1}}{M_1}\right)^2 \int_E^{M_1} dE' \; I(\lambda_D(E, E')) \left\{\sum_{\mathcal{F}} \langle \sigma v \rangle_{\mathcal{F}} \frac{dN_{\alpha(\mathcal{F}),e+}}{dE'}\right\}, \quad (18)$$

where $\tau_E = 10^{16}$ sec and ρ_{N_1} is the local DM density in the halo. In this study we use $\rho_{N_1} = 0.3$ GeV/cm^3 and $v_{e+} = c$. Possible final states directly yielded through the N_1 annihilation are expressed by $\mathcal{F}$. $dN_{\alpha(\mathcal{F}),e+}/dE'$ represents the spectrum of positrons yielded through the decay of leptons α included in the final state $\mathcal{F}$.

In this formula, the ingredients coming from astrophysics are summarized in the halo function $I(\lambda_D)$ and the positron diffusion length λ_D. They are defined by

$$I(\lambda_D) = a_0 + a_1 \tanh\left(\frac{b_1 - \ell}{c_1}\right) \left\{a_2 \exp\left(-\frac{(\ell - b_2)^2}{c_2}\right) + a_3\right\},$$

$$\lambda_D^2 = 4K_0\tau_E \left\{\frac{E^{\delta-1} - E'^{(\delta-1)}}{1 - \delta}\right\}, \quad (19)$$

where $\ell = \log_{10}(\lambda_D/\text{kpc})$. The expressions of $I(\lambda_D)$ and λ_D depend on the astrophysical model for the diffusion of positron and the halo profile [24]. In this paper we adopt med and isothermal profile for them to determine the parameters included in eq. (19). For such a model [24], parameters in λ_D are $K_0 = 0.0112$ kpc^2/Myr and $\delta = 0.70$, and others included in $I(\lambda_D)$ are

$$a_0 = 0.495, \quad a_1 = 0.629, \quad a_2 = 0.137, \quad a_3 = 0.784,$$

$$b_1 = 0.766, \quad b_2 = 0.550, \quad c_1 = 0.193, \quad c_2 = 0.296. \quad (20)$$

As addressed in several work [8], the positron flux is not crucially dependent on the astrophysical model. We choose this model for the consistency with the constraint from the diffuse gamma in the cosmic ray. We will come back to this point later.

In eq. (18) the dependence on the assumed model for particle physics is confined in the factor summed up for $\mathcal{F}$ in the E' integral. Since the annihilation cross section $\langle \sigma_2 v \rangle_{\alpha\beta}$ is proportional to $m_\alpha^2 + m_\beta^2$, the summation should be taken for

$$\mathcal{F} = (e^\pm, \tau^\mp), \ (\mu^\pm, \tau^\mp), \ (\tau^+, \tau^-), \tag{21}$$

which can yield positrons finally. This feature is caused by the flavor structure of neutrino Yukawa couplings (3). Since smaller $h_{\tau 3}$ and larger M_3 are favored from the $\mu \to e\gamma$ constraint, the N_3 contribution to the loop effect may be neglected. If we take account of these and also assume that $|y_3|$ is sufficiently small[o], the positron flux Φ_{e^+} due to the N_1 annihilation can be expressed as

$$
\begin{aligned}
\Phi_{e^+} \ \simeq \ & 1.25 \times 10^{-3} \langle \sigma_2 v \rangle \left(\frac{10^2 \ \text{GeV}}{E} \right)^2 \left(\frac{1 \ \text{TeV}}{M_1} \right)^2 \\
& \times \ \int_E^{M_1} dE' \ I(E, \ E') \left[\frac{1}{4} \frac{dN_{\mu^+, e^+}}{dE'} + \frac{3}{4} \left(\frac{dN_{\tau^+, e^+}}{dE'} + \frac{dN_{\tau^-, e^+}}{dE'} \right) \right],
\end{aligned} \tag{22}
$$

where $(\text{GeV} \cdot \text{cm}^2 \cdot \text{str} \cdot \text{sec})^{-1}$ is used for the unit of Φ_{e^+} and the total cross section $\langle \sigma_2 v \rangle (\equiv 4 \langle \sigma_{\mu^\pm \tau^\mp} \rangle)$ is determined in our extended model as

$$\langle \sigma_2 v \rangle = \frac{16}{(4\pi)^5} \frac{(\text{GeV})^2}{\left(\Delta - \frac{v_\tau^2}{4} \right)^2 + \gamma_S^2} \frac{M_1^2 m_\tau^2}{M_\eta^4 M_S^4} \left(\sum_{k=1}^2 \frac{y_1 y_k h_{\tau k}^2 M_k}{D_k} \right)^2. \tag{23}$$

Here it should be noted that we can keep the favorable feature such that the final states of the N_1 annihilation consist of heavier leptons only.[p] The fact that $e^\pm$ are not directly produced is favored to explain the Fermi-LAT data, which show no bump in the hard $e^+ + e^-$ spectrum. The directly produced $e^\pm$ tend to be much harder than indirectly produced $e^\pm$ energetically. The positron spectrum given by (22) has large contributions from τ^+ decay, which causes a softer spectrum for the final positron and electron spectrum. The decay of $\mu^\pm$ to $e^\pm$ yields much harder positron than the $\tau^\pm$ decay. The concrete model with these mixed final states seems not to have been considered in the analysis of the anomaly suggested through the PAMELA and Fermi-LAT experiments.[q]

---

[o]Under this assumption, we can safely neglect the N_3 contribution to the one-loop annihilation diagram. In this case N_1 annihilation does not yield positrons directly.

[p]Although higher order radiative corrections can induce coupling of S with the ordinary Higgs scalars, their effect is small enough to neglect them in the analysis of N_1 annihilation.

[q]Although model independent analysis for this kind of mixed final states is found in the paper by Meade et al. [8] (see Fig. 12 in it), it is not based on a concrete particle physics model.
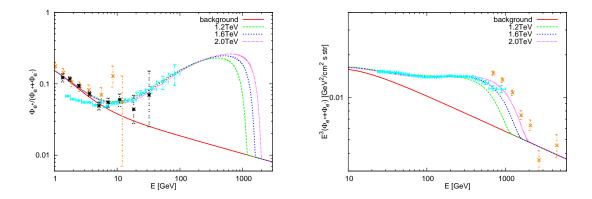
Fig. 4 Left and right panels show the predicted positron excess at the PAMELA regions and the prediction for the $e^+ + e^-$ flux at the observation regions of Fermi-LAT and H.E.S.S., respectively. In both panels, DM mass M_1 and annihilation cross section $\langle \sigma_2 v \rangle$ are fixed as $(M_1 \ (TeV), \langle \sigma_2 v \rangle \ (\text{cm}^3/\text{sec})) = (1.2, 4.1 \times 10^{-23}), (1.6, 6.7 \times 10^{-23}), (2.0, 9.2 \times 10^{-23})$. The normalization of background fluxes is taken to be $N_\Phi = 0.64$.

The energy spectrum of positron $\dfrac{dN_{\alpha,e^+}}{dE}$ can be computed by using the PYTHIA Monte Carlo code [25]. We determine the positron spectrum by fitting these simulation data for both the μ^+ and $\tau^\pm$ cases. Details of the analysis are given in Appendix B. We apply this result to eq. (22) to find the positron flux Φ_{e^+}. We fix parameters included in the cross section $\langle \sigma_2 v \rangle$ by using the ones which realize the point in the allowed region shown in Fig. 1. They are also summarized in Table 1 for the case of $M_1 = 1.6$ TeV. As expected background fluxes for positrons and electrons, we use the empirical formulas given in [26],

$$
\Phi_{e^+}^{\text{bkg}} = N_\Phi \frac{4.5 E^{0.7}}{1 + 650 E^{2.3} + 1500 E^{4.2}},
$$
$$
\Phi_{e^-}^{\text{bkg}} = N_\Phi \frac{0.16 E^{-1.1}}{1 + 11 E^{0.9} + 3.2 E^{2.15}} + N_\Phi \frac{0.70 E^{0.7}}{1 + 110 E^{1.5} + 600 E^{2.9} + 580 E^{4.2}}, \quad (24)
$$

where E should be understood in a unit of GeV and N_Φ is a normalization factor.

Using these formulas, we plot the positron fraction $\Phi_{e^+}/(\Phi_{e^+} + \Phi_{e^-})$ and the total flux of $e^+ + e^-$ scaled by E^3 in two panels of Fig. 4, respectively. In the left panel, the data points for positron excess of PAMELA [2], CAPRICE94 [28] and HEAT95 [29] are also plotted. On the other hand, the data points for the $e^+ + e^-$ flux of Fermi-LAT [3] and HESS [27] are plotted in the right panel. In this figure $\langle \sigma_2 v \rangle$ is fixed to make the positron flux Φ_{e^+} to realize a good fit to the data of PAMELA and Fermi-LAT for each

M_1 value. This figure shows that the flux of positrons and electrons predicted from the annihilation of N_1 in this extended model can give rather good fits with these experimental data. Especially, the predicted flux fits well both data of the PAMELA and Fermi-LAT experiments for $M_1 = 1.6$ TeV and $\langle \sigma_2 v \rangle = 6.7 \times 10^{-23}$ cm^3/sec. This value of $\langle \sigma_2 v \rangle$ can be realized by the parameter sets in case (ii) given in Table 1. If we apply this information for M_1 to Fig. 1, we can predict the value of $Br(\mu \to e\gamma)$ and $Br(\tau \to \mu\gamma)$. The figure shows that the predicted value for $\mu \to e\gamma$ is within the reach of the MEG experiment [30]. Thus, lepton flavor violating processes could be a crucial probe for this model.

Annihilation of the DM can cause additional contributions to the cosmic gamma ray. In fact, if hard charged leptons are produced as the final states of the DM annihilation, high energy photons are also produced through several processes. One of their origin is the inverse Compton scattering of positrons with CMB, star light and interstellar photon [31]. The other ones are final state radiation or internal radiation [33]. The gamma ray flux expected from the former one does not depend on the particle physics model as long as the positron flux data presented by PAMELA is assumed. It can be used as a crucial constraint on the model. Since the gamma ray flux caused by the latter ones depends on the adopted particle physics model, the predicted photon spectrum can be used to discriminate the model from others on the basis of the deviation of the photon spectrum from the one of background in the future observation.

In the present scenario, the DM has mass of $O(1)$ TeV and it can decay into $\tau^{\pm}$. Thus, substantial constraints are expected to be imposed by the gamma from the former origin and also the gamma produced through the decay of π^0 which comes from the $\tau^{\pm}$ decay. These give strong constraints on the gamma ray flux at higher energy regions. Various studies related to this issue have been done in the model independent way or in the fixed models [31, 34, 22]. The constraints obtained from analyses of the first year of Fermi γ-ray observations are also given in [35]. Their results for the gamma ray flux associated with the DM annihilation into charged lepton pairs are applicable to our model to examine the consistency with the diffuse gamma ray observations. They show that the galactic diffuse gamma data constrain the assumed DM halo profile severely. Only the restricted halo profile called isothermal seems to be consistent with the observations. In fact, following the study by Cirelli *et al.* in [35] for the cases with the final states $\mu^+\mu^-$ and $\tau^+\tau^-$ for the DM with mass around 1.6 TeV, the DM annihilation cross section $\langle \sigma v \rangle$ is shown to be less

than 6×10^{-23} cm^3/sec and 1×10^{-22} cm^3/sec, respectively. Papucci *et al.* in [35] gives much stronger constraints for the $\tau^+\tau^-$ case. The results in this section show that our model can satisfy these constraints for $\mu^+\mu^-$ but the situation seems to be marginal for the $\tau^+\tau^-$ case. Thus, the present model may be considered to work well in the isothermal profile, although this type of halo profile is considered to be disfavored by the N-body simulation. We also note that the diffuse neutrino flux satisfies the present observational constraints [31, 32].

4 Summary

The radiative seesaw model is a simple and interesting extension of the SM by an inert doublet scalar and singlet fermions. It can give the origin of both small neutrino masses and DM consistently. However, if we try to explain the positron excess observed by the PAMELA experiment on the basis of the DM annihilation in this model, an extremely large boost factor for the annihilation cross section is required. In this paper we have proposed a simple extension of the model by introducing a singlet scalar. In this extended model, the DM annihilation cross section can be enhanced in the present Galaxy through the Breit-Wigner resonance without disturbing the features in the original model, which are favored by the neutrino masses, the lepton flavor violating processes and the DM relic abundance. However, it should be noted that the mass of the singlet scalar has to be finely tuned at the level of $O(10^{-6})$ for this enhancement. Final states of DM annihilation are composed of heavier leptons only and the ratio of μ^+ and $\tau^\pm$ contribution to the annihilation cross section is 1 to 3. As a result of these features, the data for the positron and electron flux observed by PAMELA and Fermi-LAT are well explained in this extended model as long as the coannihilation among N_k occurs. It is interesting that these results are closely related to the flavor structure of neutrino Yukawa couplings, which induces tri-bimaximal mixing.

This extended model may be checked through the study of lepton flavor violating processes such as $\mu \to e\gamma$ in the MEG experiment and others in near future. The cosmic positron and electron flux at higher energy regions may be clarified by the future CALET experiment, which can observe $e^\pm$ flux up to 10 TeV [36]. Viability of the model may also be confirmed through this experiment. Although the diffuse gamma ray flux imposes

severe constraints on the model, they could be consistent as long as the specific halo density profile called the isothermal profile is assumed. Detailed knowledge on the density profile of the DM halo seems to be required to judge the validity of the explanation given here for the anomaly reported by PAMELA and Fermi-LAT.

Appendix A

In order to study the stability of the scalar potential, we need the renormalization group equations (RGEs) for the coupling constants included in the scalar potential V. This model is an extension of the SM with three singlet fermions N_k and one doublet scalar η. Thus, the RGEs are similar to the ones of the ordinary two doublet Higgs model. However, we need to take account of the effect of large neutrino Yukawa couplings $h_{\alpha k}$, which are assumed to satisfy the relation (3).

If we assume the existence of the hidden sector gauge interaction mentioned in the text, invariance of $\mathcal{L}_N$ restricts the representation of N_k and η to be an adjoint representation of SU(N) or a doublet of SU(2), for example. In case of the adjoint representation, scalar potential V should be modified. No anomaly problem appears in both cases. However, if we note that one-loop diagrams with internal lines of N_k and η have additional group theoretical factor dim(R), we find that the latter is favored from the constraints of lepton flavor violating processes.

To prepare RGEs applicable to this extended situation, we assume that N_k and η are singlets ($N = 1$) or doublets ($N = 2$) of a hidden gauge symmetry SU(2). All SM fields are singlets under this group. A set of relevant RGEs can be written in the following form [37]:

$$16\pi^2\frac{d\lambda_1}{dt} = 24\lambda_1^2 + 2N\lambda_3^2 + N\lambda_4^2 + 2N\lambda_3\lambda_4 + 12\lambda_1 h_t^2 - 6h_t^4 + \kappa_\phi^2,$$

$$16\pi^2\frac{d\lambda_2}{dt} = 8(N+2)\lambda_2^2 + 2\lambda_3^2 + \lambda_4^2 + 2\lambda_3\lambda_4 + 4\lambda_2\left[2\left(h_{\tau1}^2 + h_{\tau2}^2 + \frac{3}{2}h_{\tau3}^2\right) - 3C_2(N)g_h^2\right]$$

$$-8\left((h_{\tau1}^2 + h_{\tau2}^2)^2 + \frac{9}{4}h_{\tau3}^4\right) + \frac{3(N-1)(N^2+2N-2)}{4N^2}g_h^4 + \kappa_\eta^2,$$

$$16\pi^2\frac{d\lambda_3}{dt} = 4\Big(3\lambda_1\lambda_3 + (2N+1)\lambda_2\lambda_3 + \lambda_1\lambda_4 + N\lambda_2\lambda_4\Big) + 4\lambda_3^2 + 2\lambda_4^2$$

$$+2\lambda_3\left[3h_t^2 + 2\left(h_{\tau1}^2 + h_{\tau2}^2 + \frac{3}{2}h_{\tau3}^2\right) - 3C_2(N)g_h^2\right] + 2\kappa_\phi\kappa_\eta,$$

$$16\pi^2\frac{d\lambda_4}{dt} = 2\lambda_4\left[2\left(\lambda_1 + \lambda_2 + 2\lambda_3 + \lambda_4\right) + 3h_t^2 + 2\left(h_{\tau1}^2 + h_{\tau2}^2 + \frac{3}{2}h_{\tau3}^2\right) - 3C_2(N)g_h^2\right],$$

$$16\pi^2\frac{d\kappa}{dt} = 20\kappa^2 + 2\kappa_\phi^2 + 2N\kappa_\eta^2 + 8N\sum_{k=1}^{3}(\kappa|y_k|^2 - 4|y_k|^4),$$

$$16\pi^2\frac{d\kappa_\phi}{dt} = 12\kappa_\phi\lambda_1 + 4N\kappa_\eta\lambda_3 + 2N\kappa_\eta\lambda_4 + 8\kappa\kappa_\phi + 4\kappa_\phi^2 + 4N\kappa_\phi\sum_{k=1}^{3}|y_k|^2 + 6\kappa_\phi h_t^2,$$

$$
16\pi^2 \frac{d\kappa_\eta}{dt} = (8N+4)\kappa_\eta\lambda_2 + 4\kappa_\phi\lambda_3 + 4\kappa_\phi\lambda_4 + 8\kappa\kappa_\eta + 4\kappa_\eta^2 + 4\kappa_\eta\left(h_{\tau 1}^2 + h_{\tau 2}^2 + \frac{3}{2}h_{\tau 3}^2\right)
$$

$$
+4N\kappa_\eta\sum_{k=1}^{3}|y_k|^2 - 32\left(h_{\tau 1}^2|y_1|^2 + h_{\tau 2}^2|y_2|^2 + \frac{3}{2}h_{\tau 3}^2|y_3|^2\right) - 6C_2(N)\kappa_\eta g_h^2,
$$

$$
16\pi^2 \frac{dh_{\tau i}}{dt} = h_{\tau i}\left((N+4)(h_{\tau 1}^2 + h_{\tau 2}^2) + 3h_{\tau 3}^2 + 2|y_i|^2 - 3C_2(N)g_h^2\right) \quad (i=1,2),
$$

$$
16\pi^2 \frac{dh_{\tau 3}}{dt} = h_{\tau 3}\left(2(h_{\tau 1}^2 + h_{\tau 2}^2) + \frac{3}{2}(N+4)h_{\tau 3}^2 + 2|y_3|^2 - 3C_2(N)g_h^2\right),
$$

$$
16\pi^2 \frac{dy_i}{dt} = y_i\left(8|y_i|^2 + 2N\sum_{k=1}^{3}|y_k|^2 + 2h_{\tau i}^2(2+\delta_{3i})\right) \quad (i=1,2,3),
$$

$$
16\pi^2 \frac{dh_t}{dt} = h_t\left(\frac{9}{2}h_t^2 - 8g_3^2\right),
$$

$$
16\pi^2 \frac{dg_h}{dt} = \frac{g_h^3}{3}\left(-11N + \sum_{N_k,\eta}2T(N)\right),
$$

$$
16\pi^2 \frac{dg_3}{dt} = -7g_3^3, \tag{25}
$$

where $C_2(n)$ and $T(n)$ stand for values of the second order Casimir operators defined by $\sum_a T^a T^a = C_2(n)\mathbf{1}$ and $\mathrm{tr}(T^a T^b) = T(n)\delta^{ab}$ for SU(n) generators T^a in the fundamental representation. Thus, $g_h = 0$ for the $N=1$ case, and $C_2(2) = \frac{3}{4}$ and $T(2) = \frac{1}{2}$ for the $N=2$ case, respectively. In these RGEs we take account of the contributions to β-functions only from the top Yukawa coupling h_t, the neutrino Yukawa coupling $h_{\alpha k}$, the strong gauge coupling g_3 and the hidden gauge coupling g_h except for the couplings in the scalar potential. Since the β-function of λ_5 is proportional to λ_5 due to the symmetry discussed in the text, it is kept sufficiently small to be neglected.

Appendix B

In the present model the final state positron is yielded as a consequence of μ^+ and $\tau^\pm$ decay. We determine the energy spectrum of such positrons by using the PYTHIA Monte Carlo code [25]. If we write an expectation value of the number of this yielded positron per the decay of $\alpha(=\mu^+,\tau^\pm)$ as N_{α,e^+}, PYTHIA gives the positron spectrum $\frac{dN_{\alpha,e^+}}{dE}$. The spectrum obtained from this simulation is shown in Fig. 5, where the result for the $\alpha = \mu^+$ is plotted in the left panel and the one for $\alpha = \tau^\pm$ pair is plotted in the right panel. We find from these figures that the positron produced through the decay of $\tau^\pm$ is softer than the one for μ^+ as mentioned in the text.

In order to fix their empirical formulas approximately, each data set in Fig. 5 are fitted
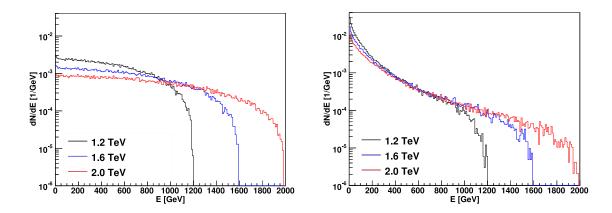
Fig. 5 The energy spectrum $\frac{dN_{\alpha,e^+}}{dE}$ obtained for the DM mass $M_1 = 1.2,\ 1.6,\ 2.0$ TeV by simulation. Left and right panels show the positron spectrum obtained from the decay of the μ^+ and $\tau^\pm$ pair, respectively.

by using the functions

$$\frac{dN_{\alpha,e^+}}{dE} = \sum_{n=0}^{2} \frac{d_n (M_1 - E)^{1/2}}{(E + E_0)^n} \tag{26}$$

where E_0 is a constant and E should be understood in a GeV unit. As results of this fitting, we find that the coefficients d_n in the above fitting functions should take the values shown in Table 2. We have $N_{\mu^+,e^+} = 1$, $N_{\tau^\pm,e^+} \sim 1.3$ by integrating the obtained spectrum. This corresponds to the fact that the decay of τ^+ is composed of various modes such as $\tau^+ \rightarrow e^+ \bar{\nu}_\tau \nu_e$, $\tau^\pm \rightarrow$ hadrons $\rightarrow e^\pm e^\pm e^\mp$, while the decay mode is dominated only by $\mu^+ \rightarrow e^+ \bar{\nu}_\mu \nu_e$ for μ^+.

particle(α)	μ^+			$\tau^\pm$		
M_1(TeV)	1.2	1.6	2.0	1.2	1.6	2.0
d_0	-2.76×10^{-3}	-3.86×10^{-3}	-2.13×10^{-3}	-2.50×10^{-6}	-1.14×10^{-6}	-7.75×10^{-7}
d_1	4.13×10^{1}	1.20×10^{2}	7.19×10^{1}	2.94×10^{-3}	1.85×10^{-3}	1.44×10^{-3}
d_2	-1.52×10^{5}	-9.26×10^{5}	-6.01×10^{5}	2.43×10^{0}	3.27×10^{0}	3.86×10^{0}
E_0	7.12×10^{3}	1.51×10^{4}	1.64×10^{4}	6.54×10^{1}	9.60×10^{1}	1.24×10^{2}

Table. 2 The coefficients d_n determined by the fitting to Fig. 5.

In the text we make the estimation of the positron flux (22) by using these positron spectra. The parameters included in the cross section $\langle \sigma_2 v \rangle$ is determined by a point in the allowed regions (on the red solid line) shown in Fig. 1. Other parameters Δ and y_k relevant only to the N_1 annihilation at the present Galaxy are fixed to make $\langle \sigma_2 v \rangle$ a suitable value $O(10^{-23})$ cm^3/sec for the explanation of PAMELA data. They are summarized

in Table 1 in the case of $M_1 = 1.6$ TeV.

References

[1] D. N. Spergel *et al.* [WMAP Collaboration], Astrophys. J. **148**, 175 (2003); E. Komatsu *et al.* [WMAP Collaboration], Astrophys. J. Suppl. **180**, 330 (2009); M. Tegmark, *et al.* [SDSS Collaboration], Phys. Rev. **D69**, 103501 (2004).

[2] O. Adriani *et al.* [PAMELA Collaboration], Nature **458**, 607 (2009).

[3] A. A. Abdo, *et al.* [Fermi-LAT Collaboration], Phys. Rev. Lett. **102**, 181101 (2009).

[4] J. Chen *et al.*, Nature **456**, 362 (2008).

[5] F. Takayama and M. Yamaguchi, Phys. Lett. **B485**, 388 (2000); A. Ibarra and D. Tran, JCAP **0807**, 002 (2008); JCAP **0902** (2009) 021; K. Ishiwata, S. Matsumoto and T. Moroi, Phys. Rev. **D78**, 063505 (2008); JHEP **0905**, 110 (2009); P. f. Yin, Q. Yuan, J. Liu, J. Zhang, X. j. Bi and S. h. Zhu, Phys. Rev. **D79**, 023512 (2009); K. Hamaguchi, S. Shirai and T. T. Yanagida, Phys. Lett. **B673**, 247 (2009); E. Nardi, F. Sannino and A. Strumia, JCAP **0901**, 043 (2009); A. Arvanitaki, S. Dimopoulos, S. Dubovsky, P. W. Graham, R. Harnik and S. Rajendran, Phys. Rev.**D79**, 105022 (2009); Phys. Rev. **D80**, 055011 (2009); I. Gogoladze, R. Khalid, Q. Shafi and H. Yuksel, Phys. Rev. **D79**, 055019 (2009); S. Shirai, F. Takahashi and T. T. Yanagida, Phys. Lett. **B680**, 485 (2009).

[6] H. Fukuoka, J. Kubo and D. Suematsu, Phys. Lett. **B678**, 401 (2009).

[7] M. Cirelli, R. Franceschini and A. Strumia, Nucl. Phys. **B800**, 204 (2008); I. Cholis, L. Goodenough, D. Hooper, M. Simet and N. Weiner, Phys. Rev. **D80**, 123511 (2009); M. Lattanzi and J. Silk, Phys. Rev. **D79**, 083523 (2009); J. March-Russell and S. M. West, arXiv:0812.0559 [astro-ph]; V. Barger, W.-Y. Keung D. Marfatia and G. Shaughnessy, Phys. Lett. **B672**, 141 (2009); M. Cirelli and A. Strumia, arXiv:0903.3381 [hep-ph]; L. Bergström, J. Edsjö and G. Zaharijas, Phys. Rev. Lett. **103**, 031103 (2009); D. Feldman, Z. Liu, P. Nath and B. D. Nelson, Phys. Rev. **D80**, 075001 (2009).

[8] M. Cirelli, M. Kadastik, M. Raidal and A. Strumia, Nucl. Phys. **B813**, 1 (2009); P. Meade, M. Papucci, A. Atrumia and T. Volansky, Nucl. Phys. **B831**, 178 (2010).

[9] E. Ma, Phys. Rev. **D73**, 077301 (2006)

[10] J. Kubo, E. Ma and D. Suematsu, Phys. Lett. **B643**, 336 (2006); D. Suematsu, Eur. Phys. J. **C56**, 379 (2008); D. Aristizabal Sierra, J. Kubo, D. Restrepo, D. Suematsu and O. Zepata, Phys. Rev. **D79** (2009) 013011.

[11] J. Kubo and D. Suematsu, Phys. Lett. **B643**, 336 (2006).

[12] Q.-H. Cao, E. Ma and G. Shaughnessy, Phys. Lett. **B673**, 152 (2009).

[13] D. Suematsu, T. Toma and Y. Yoshida, Phys. Rev. **D79**, 093004 (2009).

[14] E. Ma and M. Raidal, Phys. Rev. Lett. **87**, 011802 (2001).

[15] K. Griest, M. Kamionkowski and M. S. Turner, Phys. Rev. **D41**, 3565 (1990)

[16] K. Griest and D. Seckel, Phys. Rev. **D43**, 3191 (1991).

[17] M. L. Brooks *et al.* [MEGA Collaboration], Phys. Rev. Lett. **83**, 1521 (1999); B. Aubert *et al.* [BABAR Collaboration], Phys. Rev. Lett. **95**, 041802 (2005).

[18] K. S. Babu and E. Ma, Int. J. Mod. Phys. **A23**, 1813 (2008).

[19] D. Feldman, Z. Liu and P. Nath, Phys. Rev. **D79**, 063509 (2009); M. Ibe, H. Murayama and T.T. Yanagida, Phys. Rev. **D79**, 095009 (2009).

[20] P. Gondolo and G. Gelmini, Nucl. Phys. **B360**, 145 (1991).

[21] J. L. Feng, M. Kaplinghat and H.-B. Yu, Phys. Rev. Lett. **104**, 151301 (2010); arXiv:1005.4678 [hep-ph].

[22] G. Hüst, A. Hektor and M. Raidal, Astron. Astrophys. **505**, 999 (2009); M. Cirelli, F. Iocco and P. Panci, JCAP **0910**, 009 (2009).

[23] J. Hisano, S. Matsumoto, O Saito and M. Senami, Phys. Rev. **D73**, 055004 (2006).

[24] T. Delahaye, R. Lineros, F. Donato, N. Fornengo and P. Salati, Phys. Rev. **D77**, 063527 (2008).

[25] T. Sjostrand, S. Mrenna and P. Skands, Comput. Phys. Commun. **178**, 852 (2008), (arXiv:0710.3820 [hep-ph]), http://www.thep.lu.se/~torbjorn/Pythia.html

[26] E. A. Baltz and J. Edsjö, Phys. Rev. **D59**, 023511 (1998).

[27] F. Aharonian et al., [H.E.S.S. Collaboration], Phys. Rev. Lett. **101**, 261104 (2008).

[28] M. Boeio et al., [CAPRICE Collaboration], Astrophys. J. **532**, 653 (2000).

[29] S. W. Barwick et al., [HEAT Collaboration], Astrophys. J. **482**, L191 (1997).

[30] J. Adam *et al.* [MEG Collaboration], arXiv:0908.2594.

[31] G. Bertone, M. Cirelli, A. Strumia and M. Taoso, JCAP **03**, 009 (2009); M. Cirelli and P. Panci, Nucl. Phys. **B821**, 399 (2009).

[32] J. Hisano, M. Kawasaki, K. Kohri and K. Nakayama, Phys. Rev. **D79**, 043516 (2009).

[33] L. Bergström, T. Bringmann, M. Eriksson and M. Gustafsson, Phys. Rev. Lett. **95**, 241301 (2005); M. Gustafsson, E. Lundström, L. Bergström, and J. Edsjö, Phys. Rev. Lett. **99**, 041301 (2007); T. Bringmann, L. Bergström and J. Edsjö, JHEP **01**, 049 (2008); L. Bergström, T. Bringmann and J. Edsjö, Phys. Rev. **D78**, 103520 (2008); V. Barger, Y. Gao, W.-Y. Keung, D. Marfatia and G. Shaughnessy, Phys. Lett. **B678**, 283 (2009); V. Barger, Y. Gao, W.-Y.Keung and D. Marfatia, Phys. Rev. **D80**, 063537 (2009).

[34] M. Kawasaki, K. Kohri and K. Nakayama, Phys. Rev. **D80**, 023517 (2009); S. Profumo and T.E. Jeltema, JCAP **0907**, 020 (2009); A.V. Belikov and D. Hooper, Phys. Rev. **D81**, 043505 (2010).

[35] M. Cirelli, P. Panci and P. D. Serpico, arXiv:0912.0663 [astro-ph.CO]; M. Papucci and A. Strumia, arXiv:0912.0742 [hep-ph].

[36] S. Torii, J. Phys. Soc. Jpn. **78** Suppl A, 68 (2009).

[37] T. P. Cheng, E. Eichten and L.-F. Li, Phys. Rev. **D9**, 2259 (1974).